Synthetic Seismograms for a Synthetic Earth
Long-Period P- and S-wave traveltime variations can be explained by temperature alone

Bernhard S. A. Schuberth[1], Christophe Zaroli[2] and Guust Nolet[3]

1) Dept. of Earth and Environmental Sciences, Ludwig-Maximilians-University Munich, Germany. 2) Institute de Physique du Globe de Strasbourg (Université de Strasbourg/EOST), France. 3) Géoazur, Université de Nice – Sophia Antipolis, France. Contact: mail@bernhard-schuberth.de

LUDWIG-MAXIMILIANS-UNIVERSITÄT MÜNCHEN — GeoAzur TERRE · OCÉAN · ESPACE — MARIE CURIE ACTIONS
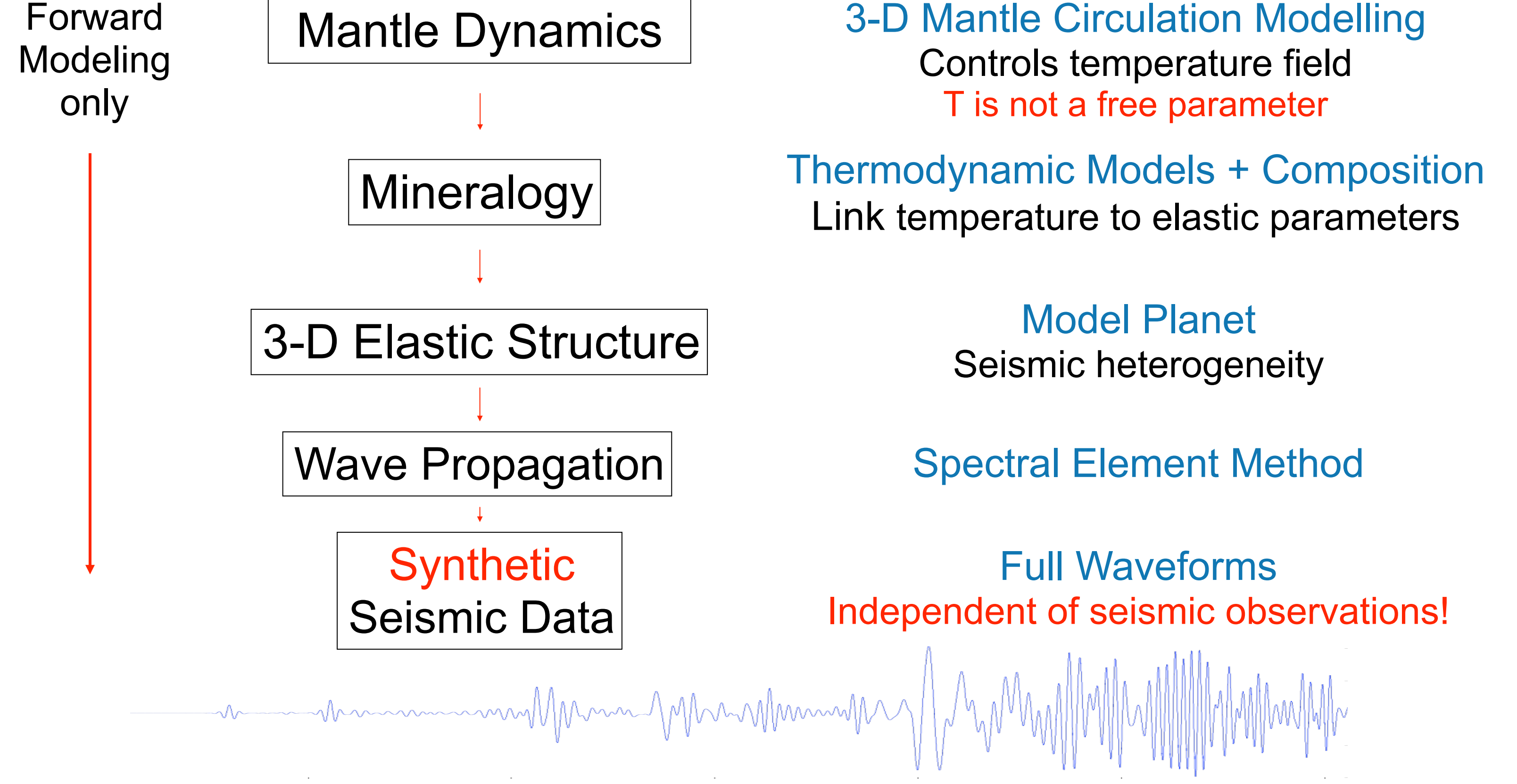
1. Abstract

Current interpretations of seismic observations typically argue for significant chemical heterogeneity being present in the two large low shear velocity provinces under Africa and the Pacific. Recently, however, it has been suggested that large lateral temperature variations in the lowermost mantle resulting from a strong thermal gradient across D" may provide an alternative explanation. In case of a high heat flux from the core into the mantle, the magnitude of shear wave velocity variations in tomographic models can be reconciled with isochemical whole mantle flow and a pyrolite composition (see Fig. 1). So far, the hypothesis of strong core heating has been tested in a consistent manner only against tomographic S-wave velocity models, but not against P-wave velocity models.

Here, we explore a new approach to assess geodynamic models and test the assumption of isochemical whole mantle flow with strong core heating directly against the statistics of observed traveltime variations of both P and S waves. Using a spectral element method, we simulate 3-D global wave propagation for periods down to 10 s in synthetic 3-D elastic structures derived from a geodynamic model. Seismic heterogeneity is predicted by converting the temperature field of a high-resolution mantle circulation model (MCM) into seismic velocities using thermodynamic models of mantle mineralogy. Being based on forward modelling only, this approach avoids the problems of limited resolution and non-uniqueness inherent in tomographic inversions while taking all possible finite-frequency effects into account. Capturing the correct physics of wave propagation allows for a consistent test of the assumption of high core heat flow against seismic data.

2. Approach

Forward Modeling only

Mantle Dynamics → Mineralogy → 3-D Elastic Structure → Wave Propagation → Synthetic Seismic Data

3-D Mantle Circulation Modelling
Controls temperature field
T is not a free parameter

Thermodynamic Models + Composition
Link temperature to elastic parameters

Model Planet
Seismic heterogeneity

Spectral Element Method

Full Waveforms
Independent of seismic observations!

3. Mantle Circulation Model

Mass, energy and momentum conservation
in 3-D spherical shell

High numerical resolution
model Earth-like convective vigour
Ra ~10^9 → realistic temperature variations

Plate motion history
as surface boundary condition

Simple 3-layer viscosity profile
10^{23}, 10^{21}, 10^{23} Pa s in the lithosphere, upper & lower mantle, respectively

High CMB temperature of 4200 K
→ high core heat flux of ~10 TW

Seismic velocities linked to temperature
→ full non-linear temperature dependence
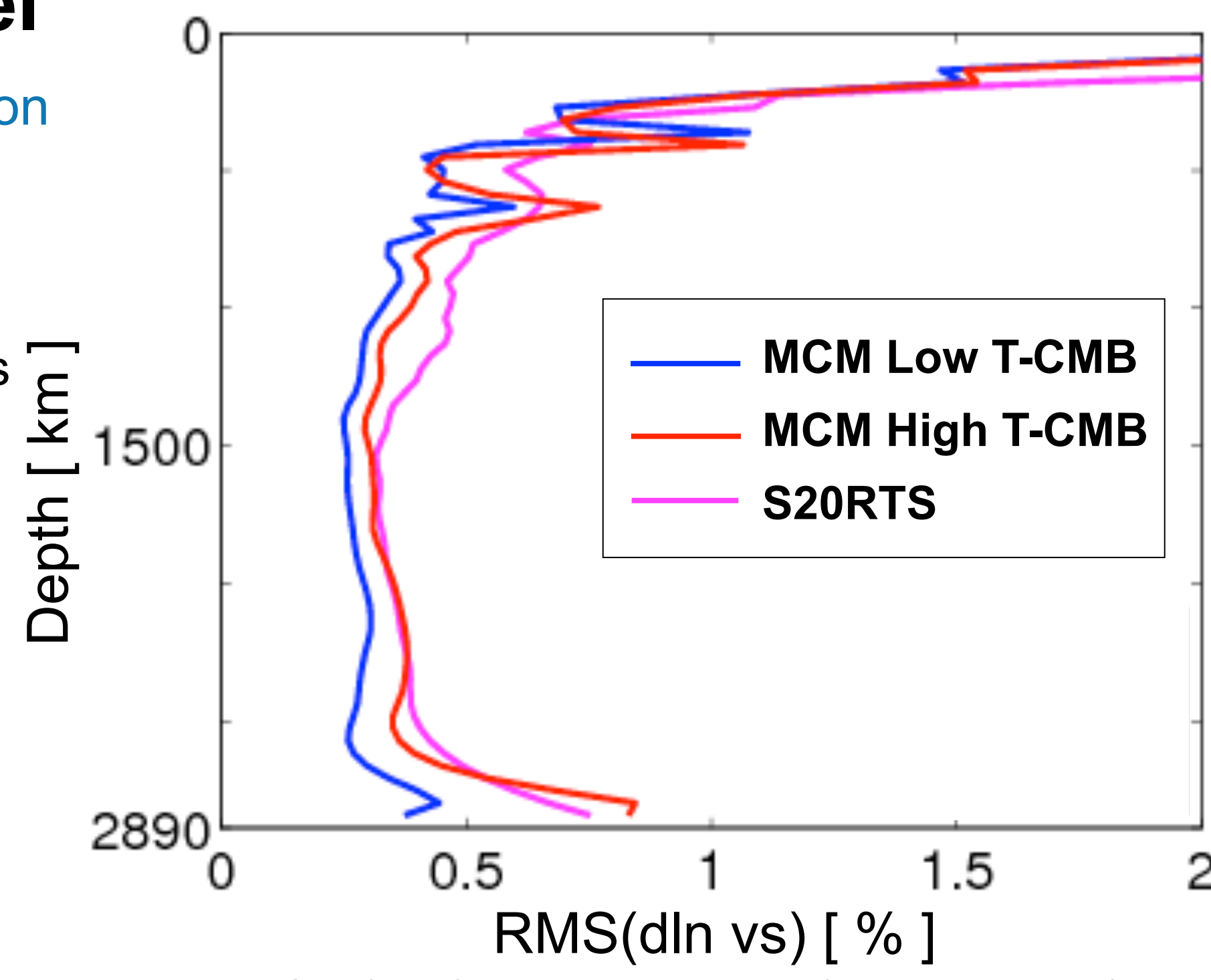
Isochemical with a pyrolite composition

Fig. 1. RMS profiles of relative variations in Vs for tomographically filtered mantle circulation models with (blue) a CMB temperature of 2900 K and (red) 4200K. The magenta line shows the RMS profile of S20RTS [Ritsema et al., 2004] for comparison. Modified after [Schuberth et al. 2009a].

4. Wave Propagation in a Synthetic Earth

Wavefield with 10 s shortest period
SPECFEM3D Globe
Komatitsch & Tromp 2002a

Traveltime delays
Full waveform cross-correlation at 15 s
Finite-frequency interpretation

3-D mantle heterogeneity only
1-D crust
no attenuation, anisotropy, topography, etc.

Homogeneous data coverage
17 earthquakes
42250 equidistant virtual station
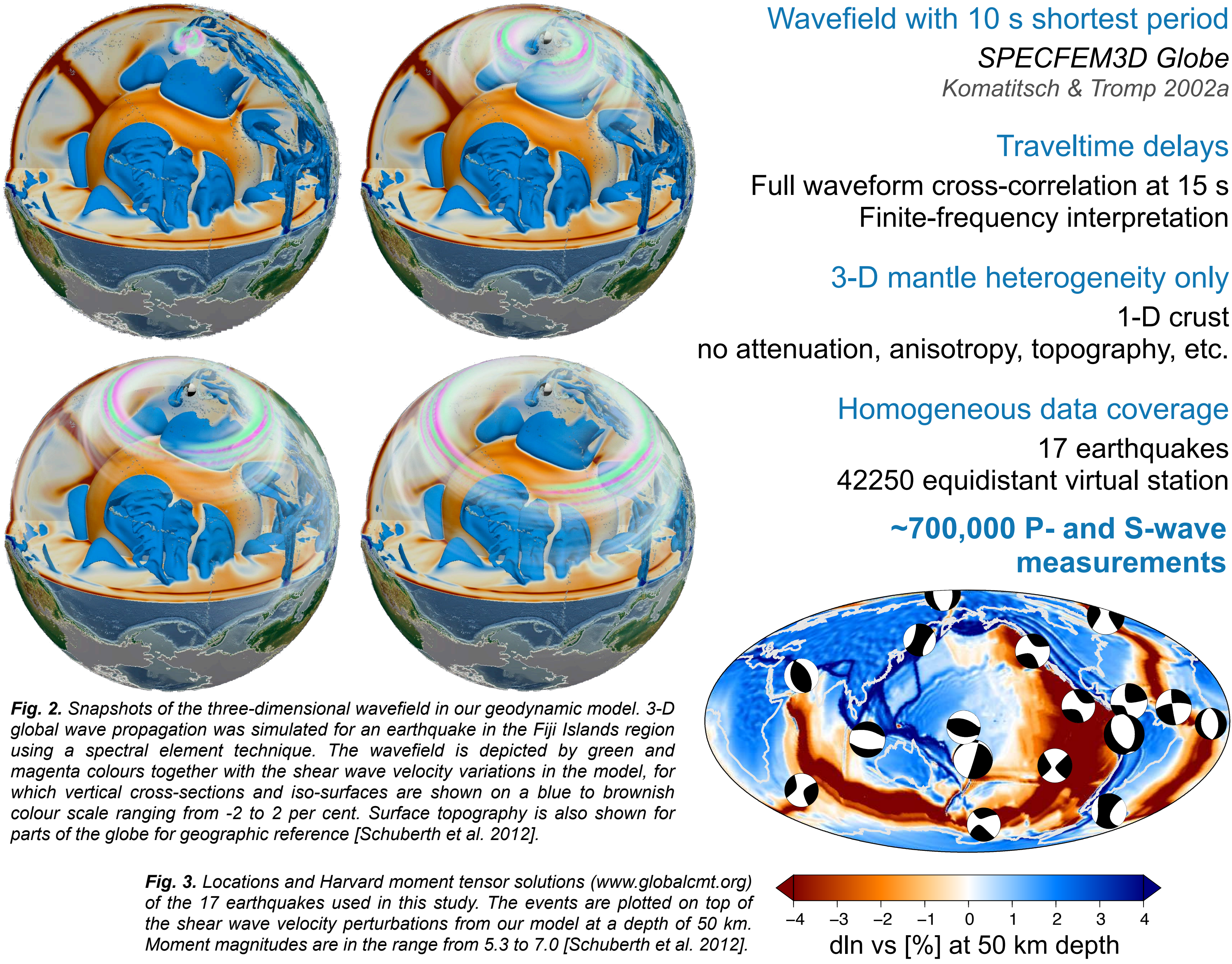**~700,000 P- and S-wave measurements**

Fig. 2. Snapshots of the three-dimensional wavefield in our geodynamic model. 3-D global wave propagation was simulated for an earthquake in the Fiji Islands region using a spectral element technique. The wavefield is depicted by green and magenta colours together with the shear wave velocity variations in the model, for which vertical cross-sections and iso-surfaces are shown on a blue to brownish colour scale ranging from -2 to 2 per cent. Surface topography is also shown for parts of the globe for geographic reference [Schuberth et al. 2012].

Fig. 3. Locations and Harvard moment tensor solutions (www.globalcmt.org) of the 17 earthquakes used in this study. The events are plotted on top of the shear wave velocity perturbations from our model at a depth of 50 km. Moment magnitudes are in the range from 5.3 to 7.0 [Schuberth et al. 2012].

dln vs [%] at 50 km depth

5. Synthetic Seismic Data

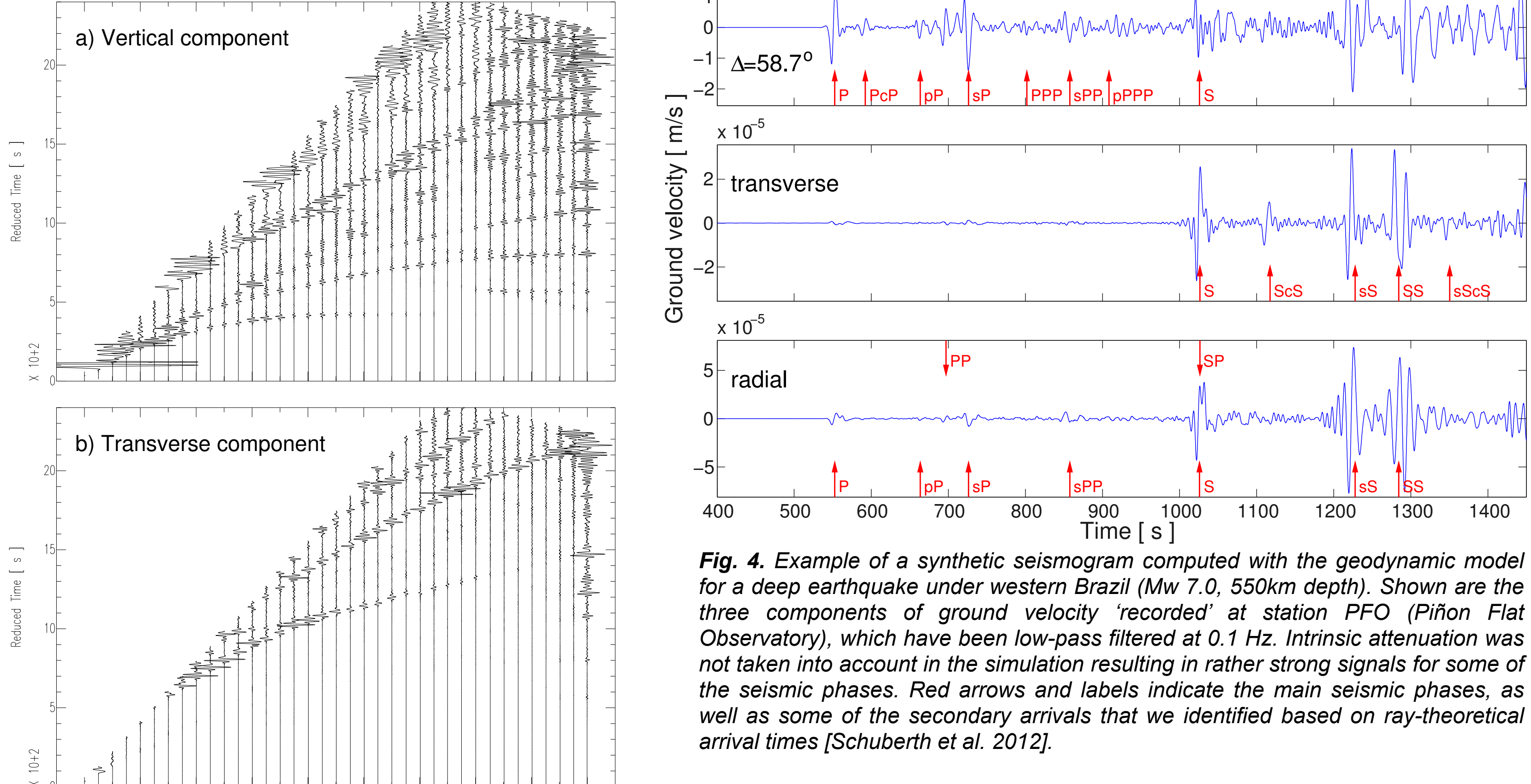a) Vertical component
b) Transverse component

Fig. 4. Example of a synthetic seismogram computed with the geodynamic model for a deep earthquake under western Brazil (Mw 7.0, 550km depth). Shown are the three components of ground velocity 'recorded' at station PFO (Piñon Flat Observatory), which have been low-pass filtered at 0.1 Hz. Intrinsic attenuation was not taken into account in the simulation resulting in rather strong signals for some of the seismic phases. Red arrows and labels indicate the main seismic phases, as well as some of the secondary arrivals that we identified based on ray-theoretical arrival times [Schuberth et al. 2012].

Fig. 5. Epicentral distance plots for an earthquake at the central Mid-Atlantic Ridge (Mw 6.2). The synthetic seismograms show ground velocity and have been low-pass filtered at 0.09 Hz to remove numerical noise below 10 s period. Surface wave energy has been removed for better visualization of body wave phases and traces have been shifted along the time axis with a dynamic delay given by 0.04 s. The dissipation of seismic energy due to intrinsic anelasticity has not been taken into account in the simulation [Schuberth et al. 2012].

Traveltime delays are dominated by the near surface structure

Centr. Mid-Atl. Ridge 2004 Mw 6.2 — Iceland 2000 Mw 6.4 — NE Coast USSR 1990 Mw 5.5 — SW Indian Ridge 2007 Mw 5.7

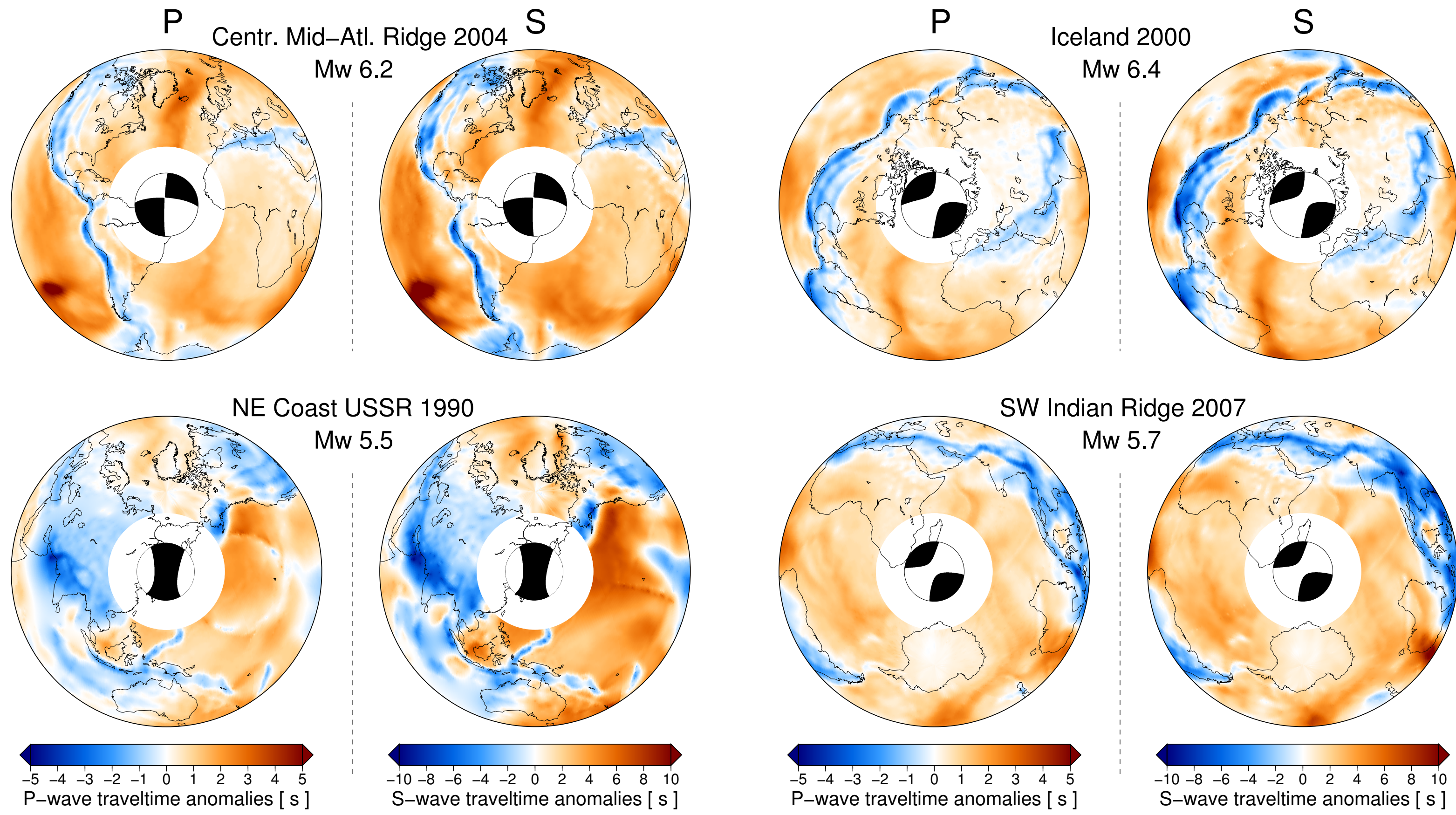P-wave traveltime anomalies [s] — S-wave traveltime anomalies [s]

Fig. 6. Maps of traveltime variations, measured by cross-correlation of full waveform synthetic seismograms. 1st and 3rd column: Traveltime variations of direct P waves for four different earthquakes. 2nd and 4th column: Same for S waves. The traveltime anomalies are plotted at the location of their respective receiver. A minimum epicentral distance range of 30° is used to guarantee a clear separation of the direct phases from later arrivals and to avoid problems due to upper-mantle triplications. Note the different colour scales for P and S waves [Schuberth et al. 2012].

6. Comparison to Observations

The statistics of long-period body wave traveltime observations show a markedly different behaviour for P and S waves: the standard deviation of P-wave delay times stays almost constant with turning depth, while that of the S-wave delay times increases strongly throughout the mantle.
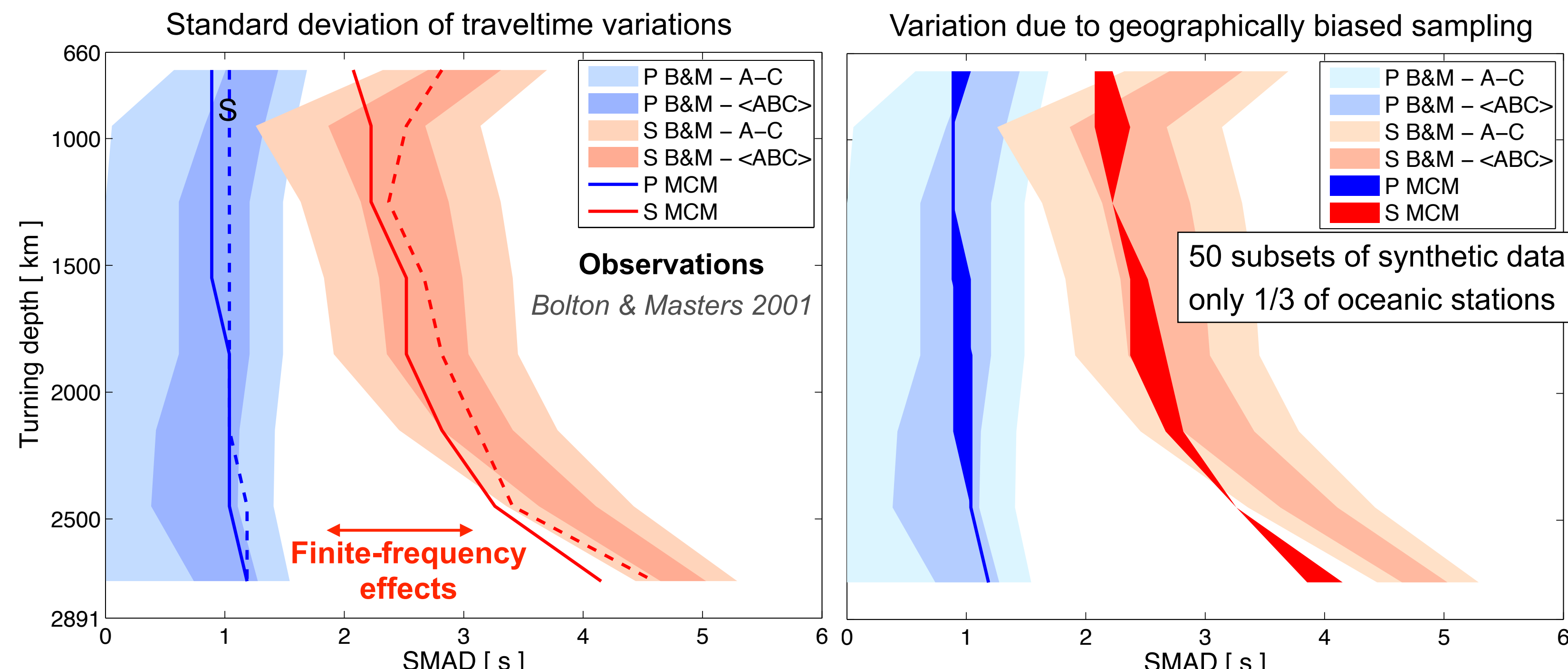

Standard deviation of traveltime variations — Variation due to geographically biased sampling

Observations *Bolton & Masters 2001*

50 subsets of synthetic data only 1/3 of oceanic stations

Finite-frequency effects

Fig. 7. Left: Comparison of the standard deviation of traveltime variations in our model to that part of the standard deviation of the observations only that can be attributed to 3-D mantle heterogeneity alone. Intermediate and light shaded areas show the range of values inferred from the data of Bolton & Masters (2001). A, B and C denote measurements of different quality. Blue lines: scaled median average deviation (SMAD) of the synthetic P-wave traveltime variations. Red lines: same for S waves. SMAD curves are shown for two types of measurements: (solid lines) full waveform cross-correlation measurements and (dashed lines) 'first upswing' measurements. Note that we focus on the cross-correlation traveltime variations, as their corresponding sensitivity (i.e. banana–doughnut kernel) is well defined and allows for a direct and intuitive interpretation of the results.
Right: Dark blue and red areas show the variation of the standard deviation in our synthetic data due to a geographically biased coverage: 50 random subsets have been drawn from our data set, each time considering only 1/3 of the stations located in oceanic regions. Here, only SMAD curves calculated from the cross-correlation measurements are shown [Schuberth et al. 2012].

Surprisingly, synthetic traveltime variations computed for the isochemical MCM reproduce the different trends of P- and S-waves. This is not expected from a ray-theoretical point of view and highlights the importance of finite-frequency effects. Most importantly, the large lateral temperature variations in the lower mantle related to strong core heating are able to explain most of the standard deviation of observed P- and S-wave delay times. This is a strong indication that seismic heterogeneity in the lower mantle is likely dominated by thermal variations on the length scales relevant for long-period body waves.

7. Conclusions and Outlook

Joint forward modelling – a complementary tool to tomographic inversions.

Chemical heterogeneity is not required to explain differences between P- and S-wave traveltime variations.

Is the strong increase in R=dln(Vs)/dln(Vp) with depth and the anti-correlation of Vs and bulk sound velocity also related to wavefront healing?

What are the effects of varying the anelasticity correction and which role plays the possible existence of post-perovskite?

References

Bolton, H. & Masters, G., J. geophys. Res., 106(B7), 13 527–13 540, 2001.
Komatitsch, D. & Tromp, J., Geophys. J. Int., 149, 390–412, 2002a.
Ritsema, J., van Heijst, H.J. & Woodhouse, J.H., J. geophys. Res., 109(B2), B02302, doi:10.1029/2003JB002610, 2004.
Schuberth, B.S.A., Bunge, H.-P. & Ritsema, J., Geochem. Geophys. Geosyst., 10 (5), Q05W03, doi:10.1029/2009GC00240, 2009a.
Schuberth, B.S.A., Zaroli, C. and G. Nolet, Geophys. J. Int., 188(3), 1393-1412, doi:10.1111/j.1365-246X.2011.05333.x, 2012.